East European Journal of Physics. 3. 402-414 (2026)
DOI:10.26565/2312-4334-2026-3-37 ISSN 2312-4334

MODELING AND OPTIMIZATION VALIDATION OF Sb_2Se_3 THIN FILM SOLAR CELLS IN SCAPS-1D SOFTWARE

K.M. Kuchkarov, B.A. Ergashev, R.T. Yuldoshov, M.P. Pirimmatov, R.R. Khurramov, D.Z. Isakov, M.A. Makhmudov, Sh.M. Bobomuradov*, A.S. Matmuratov, A.I. Eshqorayev
A.S. Azimov Physical-Technical Institute, Chingiz Aytmatov Street 2B, Tashkent 100084, Uzbekistan
**Corresponding Author e-mail: sherzodbobomuradov2@gmail.com*
Received April 28, 2026; revised June 16, 2026; accepted August 3, 2026

This analytical essay discusses antimony selenide (Sb_2Se_3) as a potential candidate material to be used as a thin-film photovoltaic absorber. Sb_2Se_3 has provided significant ecological/economic benefits, including large optical absorption, an adjustable band gap of about 1.13 eV, and a lack of toxic elements. A parametric exploration was carried out in the current study based on the platform SCAPS-1D in order to identify ideal layer designs, interfaces, carrier dynamics, and band alignments. This analysis has focused on loss mechanisms which constrain photovoltaic performance in an effort to isolate and come up with strategies to inhibit Shockley-Read-Hall recombination, surface recombination, band-offset differences, and internal diffusion effects. The results provide practical suggestions for minimizing voltage losses, such as minimizing absorber/buffer thicknesses, minimizing acceptor densities, optimizing the conduction band offset as close to zero as possible, and minimizing surface recombination and defect densities.
Keywords: *Sb_2Se_3; Thin-film solar cell; SCAPS-1D; Theoretical model; Parameter optimisation; Photovoltaic efficiency*

1. INTRODUCTION

The increasing energy needs of society have created an impetus to develop different means of harnessing renewable energy through research and technology. In particular, newer photovoltaic (PV) technology represents a more effective and environmentally friendly means of tapping into solar energy; additionally, the new methods being developed also represent ways to reduce manufacturing costs while at the same time achieving extremely high photovoltaic conversion efficiency PCE. Numerous categories of thin-film solar cell (TFSC) technology have garnered significant research interest recently due to the ability to minimize material usage, increase flexibility, and achieve high efficiency [1]. Recently, TFSC materials in multiple categories such as cadmium telluride (CdTe), copper indium gallium selenide (CIGS), and perovskite have gained tremendous popularity for use in solar cells. However, each material category has some limitations, particularly regarding the long-term viability of these materials (including the toxicity of cadmium (Cd) and indium (In)). Thus, many environmentally friendly and non-toxic materials for Photovoltaic (PV) applications have been researched, including copper zinc tin sulfide (Cu_2ZnSnS_4), SnS, Cu_2O, and $CuSbSe_2$ and their chalcogenides, antimony selenide (Sb_2Se_3) as well [2]. The maximum PCE obtainable by a single-junction solar cell is 32.23%, which occurs at approximately 1.14 eV, the optimal energy bandgap for the absorbing layer based on the Shockley-Queisser model [3]. These results indicate that Sb_2Se_3 is becoming a candidate material of choice for chalcogenides to absorb Solar Energy due to its opto-electronic properties such as high electron mobility (15 cm^2/Vs), hole mobility (42 cm^2/Vs), and good bandgap [4], which ranges from 1.10 -1.30 eV depending on application. It also has very low conductivity [5], a low melting point (612ºC), and a high absorption coefficient ($> 10^5$ cm^{-1}). In addition, Sb_2Se_3 has stability as an alternate absorber material for the construction of solar cells, thus allowing compatibility with current methods of production. Studies conducted by Wen et al. [6] reported improved charge-carrier mobility for the use of Sb_2Se_3 layers produced by means of vapor transport deposition technology (VTD), yielding efficiencies as high as 7.6% for VTD-produced films. Similarly, Li et al. [7] produced oriented nanorod assemblies of Sb_2Se_3 via closed-space sublimation (CSS) on Mo electrodes, yielding efficiencies of 9.2%. Huan et al. [8] created thin-filmed Sb_2Se_3 solar cells achieving 6.53% efficiency. Lin et al. [9] fabricated glass/Mo/Sb_2Se_3/CdS/ITO/Ag solar cells by means of spray application yielding PCE of 7.43%, which was subsequently improved to 8.64% by Tang et al. [10] Given the evolving effort to optimize these performance measures the current understanding of Sb_2Se_3 based solar cells has been explored with the aid of computer simulations utilizing the SCAPS-1D software, further enhancing the understanding of photovoltaic phenomena and supporting experimental development. The SCAPS-1D program is one of the most widely used tools for modeling thin-film solar cells. It has demonstrated its ability to accurately predict how a given solar cell will perform. With SCAPS-1D, electrical and optical properties of Sb_2Se_3 solar cells were able to be accurately simulated and the effects of material properties, layer thicknesses, doping levels, and defect densities on device performance were studied. As such, this simulation approach can save significant time and money compared to traditional experimental trial-and-error approaches, while also increasing understanding of the physical processes that limit device performance.

Cite as: K.M. Kuchkarov, B.A. Ergashev, R.T. Yuldoshov, M.P. Pirimmatov, R.R. Khurramov, D.Z. Isakov, M.A. Makhmudov, Sh.M. Bobomuradov, A. Matmuratov, A.I. Eshqorayev, East Eur. J. Phys. 3, 402 (2026), https://doi.org/10.26565/2312-4334-2026-3-37

In the research of Lin Ling-yang, the optimal layer thickness, defect density, and carrier mobility were identified by SCAPS-1D for the Sb_2Se_3/CdS solar cell structure to improve the cell efficiency, based on the SCAPS-1D parameters effective PCE. The solar cell structure has very promising attributes, including abundant material sources, low cost, and nontoxicity, as well as very effective construction of the absorber layer (600 nm) and buffer layer (60 nm), improved hole mobility, and low defect density. The PCE discovered in this research was 16.5% and consisted of a study of the effect of back contact work function [11]. The new Sb_2Se_3 based solar cell structure proposed by Baig and Faisal along with other co-authors used Eco-friendly and inexpensive materials to achieve a solar cell efficiency of 13.2 per cent. The researchers substituted the heavy-metal toxic elements Cd and Pb with Cu_2O as an HTM, In_2S_3 buffer layer, and a layer of CNT as a back contact to form the innovative new solar cell structure [12]. The effect of interface passivation on the performance of Sb_2Se_3 solar cells was also investigated in research by Chen et al. [13], who found that interface passivation was able to remove some defects and therefore, that SnO_2 was an important factor due to its ability to reduce defects and increase cell performance, a key aspect for practical use of the cells. Research by Sheikh et al. [14] indicated that CdS/Sb_2Se_3 devices with a 1 μm absorber thickness achieved a PCE of 29.35%. Similarly, [15] ZnS/Sb_2Se_3/PEDOT:PSS devices with an absorber layer thickness of 0.8 μm achieved the same PCE, which did not take into account any influence of the defect density on the interface. A WS_2/Sb_2Se_3/Cu_2O solar cell with a 0.5 μm thick absorber layer achieved a PCE of 30.03% [16], also without the effects of defect density on the interface. Because of the interfacial layer separating the collector layer of the Sb_2Se_3 (semiconductor) from the collector contact (metal), there are less downward band bending at the Sb_2Se_3/metal junction, making it easier for electrons and holes to move through the collector layer toward the collector metal. Reducing downward band-bending at the Sb_2Se_3/metal junction will eliminate the "pinning" or locking of the Fermi energy level at this junction. Eliminating such pinning will also improve transport of holes from the absorber layer to the collector, thereby reducing the amount of carrier recombination that occurs during the illumination phase. The interfacial layer will also facilitate the movement of holes through the back contact via the smallest band gap energy difference valence band offset (VBO) between the two. Therefore, it is critical to use certain materials that are compatible with the hole transport material (HTM) and back surface field (BSF) materials to maximize the electrical and optical performance. Cu_2O, a non-toxic, abundant, and easily manufactured material has been found to serve as a suitable HTM for Sb_2Se_3 solar cells [17].

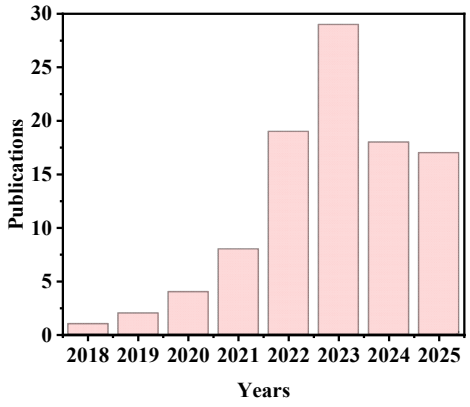

Figure 1. Publications on Sb_2Se_3 based thin-film solar cells using SCAPS-1D, categorized by years

The current modeling methods (i.e. SCAPS-1D simulations) have already demonstrated that significant improvements in power conversion efficiency for Sb_2Se_3 solar cells can be achieved by utilizing the modeling methods. Modern experimental fabrication and characterization of Sb_2Se_3 solar cells have thus been successful with the SCAPS-1D simulations of these cells. The role of absorbers, the doping levels of buffer layers, and the band alignments at the interface of thin film solar cells have all been modelled using simulations. The results obtained from the modelling of these parameters agree with the experimental values of the central electrical parameters such as PCE, V_{oc}, J_{sc} and FF. There can be discrepancies between the simulations and the experimental results due to the effects of non-ideal conditions, such as material inhomogeneity, defects at the interface, and other environmental influences. As shown in Figure 1, the publications on Sb_2Se_3 thin-film solar cells modelled using SCAPS-1D by the authors in journals indexed in SCOPUS for the period of 2018-2025.

This research paper will provide a comprehensive review of thin-film solar cells based on Sb_2Se_3 through simulation and analysis with SCAPS-1D. The significance of utilizing simulation and computation as an integral part of PV research will be discussed in depth. We will provide an in-depth description of the factors that affect the efficiency of a photovoltaic device and document new techniques (e.g., Interface engineering, control of doping level, use of machine learning, etc.) that could potentially alleviate current limitations of such devices.

2. MATERIAL PROPERTIES

Sb_2Se_3 thin films have a many beneficial properties, but their performance continues to lag behind the maximum potential performance predicted by the Shockley-Queisser (SQ) limit as the devices have yet to reach maximum attainable efficiencies. We encourage further development in three areas for improving the efficiency of Sb_2Se_3 thin film solar cells: First, better controlling the kinetics and morphology of Sb_2Se_3 precipitate growth while maintaining their high stability; second, ensuring proper alignment of the bandgap and energy bands in the device structure; and finally, minimizing recombination centers (defects at the interface and within the bulk of the material). Sb_2Se_3 belongs to A_2B_3-type isostructural compounds. These compounds are characterized by the presence of a metal A (bismuth or antimony) and a non-metal B (sulphur or selenium), and they are part of a larger family (A^{V}_{m} B^{VI}_{n}) that contains numerous compounds with similar structural arrangements. The orthorhombic stable phase of Sb_2Se_3 has orthorhombic Pbnm and Pnma crystallographic symmetry, and both of these space groups are crystallographically identical. Minor differences arise

when changing the directions of the coordinate axes. Pbnm lattice constants are a = 11.62 Å, b = 11.77 Å, c = 3.962 Å, and Pnma lattice constants are a = 11.7938 Å, b = 3.9858 Å, c = 11.6478 Å [18]. The crystal structure of Sb_2Se_3 is ribbon-like (or pseudo-1D) in its basic form, and this wrapping ribbon-like structure leads to anisotropic charge conduction and optoelectronic response of this compound, so the physicochemical stability of Sb_2Se_3, as well as the phase structure, texture, and orientation, needs to be controlled to take full advantage of its functionality.

2.1. Material Structure

The repeating structure of Sb_2Se_3 occurs as chains of $(Sb_4Se_6)_n$ between layers where van der Waals forces bind the chains together in the (010) direction, and covalent bonds hold them to form the (001) direction. The space between the ribbons was 2.98 Å, as referenced in [18]. In obtaining an effective application from the (221) direction, Sb_2Se_3 should be within 0.3-0.6 µm for optimal device use, while the diffusion distance for electrons when considering a (221) direction is only considered to be 0.3 µm, as stated in reference [5]. On the other hand, when measuring in the (001) direction the electrons can diffuse up to 1.7 µm which is five times longer than the (221) diffusion distance, as stated in reference [19].

As a result of this quasi-one-dimensional crystal system (as shown Figure 2), Sb_2Se_3 is highly anisotropic, with impediments on the trajectory of charge carriers occurring along all planes of the structure, except for one plane parallel to the c-axis (ribbon) direction. Due to limitations on carrier behavior within most of the ribbon's geometry, the carrier mobility of Sb_2Se_3 is rather poor in terms of the degree of mobility [4]. To modify the electronic characteristic properties of Sb_2Se_3, dopants such as transition metals or halogens can be introduced to produce additional energy state levels within the Sb_2Se_3 band gap, resulting in the band gap expanding or contracting depending upon the specialized dopant and doping configuration used. The electronic properties of thin film geometries also affect the size of the band gap as a result of changes in bond length and changes in the dimensions of the unit cell lattice constant, in addition to the influence of externally applied pressure, which has the potential to decrease the band gap, along with the effects of thermal expansion or contraction resulting from temperature changes.

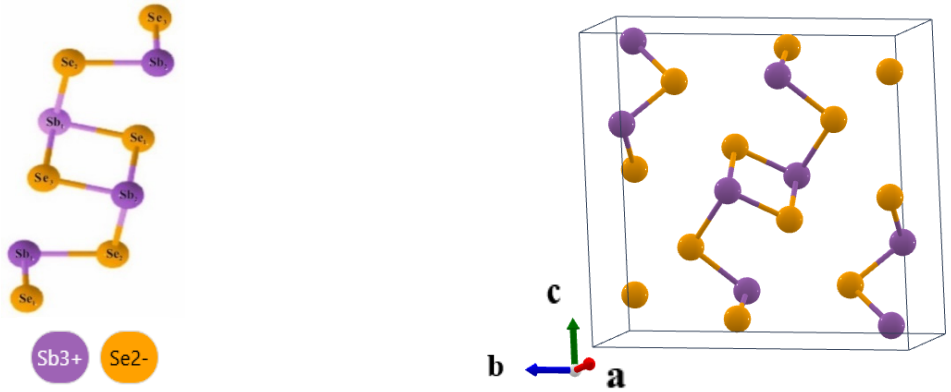

Figure 2. a) The asymmetric placement of antimony (Sb purple dots) and selenium (Se yellow dots) within the third phase of the Sb_2Se_3 compound, according to the Pbnm space group. b) An illustration of the "ribbon" configuration of the Sb_2Se_3 material system, such that dashed lines in black indicate the presence of van der Waals interactions holding together Se between different ribbons [20]

2.2. Defects in Antimony Selenide

Grain boundary defects in polycrystalline thin films were historically conceived of as recombination centers [21]. This conceptual framework is replicated from prior research on semiconductor systems such as GaAs and CdTe that exhibit similar behaviors due to their simple binary phase chemistry. It was originally assumed that the simple binary phase chemistry of Sb_2Se_3 would afford it a limited number of natural defects with respect to its management when compared with the multinanometallic systems such as CZTS/Se. Based on this assumption, it was hypothesized that there would be six intrinsic types of defects formed in this system:

(a) The two types of vacancies will exist in the form of cation vacancies (V_{Sb}) and anion vacancies (V_{Se}).

(b) The interstitials will consist of two types: cation interstitials (Sb_i) and anion interstitials (Se_i).

(c) The antisite defects will exist in the form of cation-on-anion antisites (Sb_{Se}) and anion-on-cation antisites (Se_{Sb}).

However, experimental and theoretical results indicate that the intrinsic defects in Sb_2Se_3 are far more complex than originally envisioned, and that the defect physics of this quasi-one-dimensional van der Waals material cannot be simply extrapolated from the three-dimensional covalently bonded binary photovoltaic absorbers (e.g. GaAs, CdTe).

2.3. Defect Tolerance of Photovoltaic Absorbers

There are two main reasons for the differences in defect tolerance between absorbers in photovoltaics and other types of solar cells: (1) the lack of deep traps in the gap energy region makes it a very good property of an absorber; and (2) the properties of the defects depend on the atomic position in the Q1D structure. For example, there are 3 different positions for Se atoms in a given Sb_2Se_3 ribbon (Se_1, Se_2, Se_3) but only 2 different positions for Sb in that ribbon (Sb_1, Sb_2), which means that defects in the same atomic location will have vastly different properties when considered in relation to either site.

Also, the low van der Waals strength of the $(Sb_4Se_6)_n$ chains leaves large voids between the $(Sb_4Se_6)_n$ ribbons, and as a result, defects appear in ways entirely unlike those of traditional absorbers. Such examples include cation-on-anion antisite defects (Sb_{Se}), anion-on-cation antisite defects (Se_{Sb}), and even two anions on one cation antisite defects ($2Se_{Sb}$). Thus, there are only a couple of basic defect types in this structure, but they are complicated because of the unusual structure of Sb_2Se_3. Se can be used to replace antimony's cation-anion character, resulting in Se_{Sb} and Sb_{Se} antisite defects. These defects are still debated to be acceptors or donors [22].

3. INFORMATION ABOUT THE SCAPS-1D PROGRAM

The SCAPS-1D software package was developed at Ghent University, Belgium, by Prof. Burgelman in the Electronics and Information Systems department and is a tool to evaluate the electro-mechanical properties of photovoltaic components such as solar cells, and increase their efficiency. Researchers and engineers have utilized SCAPS-1D extensively to explain the structure, material composition and working characteristics of solar cells. SCAPS-1D has applications in several areas of research: modelling of solar cells with materials including silicon (Si), CIGS, perovskites, Sb_2Se_3, etc; optimization of PCE by finding the best operating point for a solar cell and establishing how different material properties, thickness of layers, and concentrations of dopants impact the performance of the solar cell; validation of experimental results via simulation.

3.1. Main Input Parameters

The parameters that need to be entered into SCAPS-1D for solar cell modeling are as follows: Layer Thickness, Absorber and Buffer Thickness, and also the thickness of the Contact Layer.

Bandgap (E_g)

Dielectric permittivity (ε)

Electron mobility and hole mobility (μ)

Doping concentration, with n-type donor doping and p-type acceptor doping, and all that influence the electrical performance

Defect density, which includes the defect states that affect carrier recombination

Illumination intensity, or the solar irradiation intensity for example, 1 sun ≈ 1000 W/m^2

Spectral distribution of illumination (for example, AM1.5)

Temperature, being the nominal operating temperature of the device that is ~300K

Selection of the device structure (p - n junctions or heterojunctions)

Entering Parameters, such as material properties, layer thicknesses, doping concentrations, and other values

Running simulation - calculates the important electrophysical properties, such as I - V curve and quantum efficiency

Analyzing results to determine how well simulated results compare to experimental results and process optimization.

3.2. Advantage of the SCAPS-1D program

SCAPS-1D can simulate very complex multilayer structures with different semiconductor materials, as well as contacts and intermediate layers. This capability is very important for the research and optimization of different types of solar technologies, (i.e. Perovskite, Silicon, Organic, etc.) Although SCAPS-1D is fundamentally one-dimensional, it produces extremely accurate results for a wide variety of multilayered structures. SCAPS-1D allows users to model a variety of physical processes related to the operation of semiconductor devices including: the many types of recombination processes that can occur (such as Shockley-Read-Hall and surface recombination), quantum mechanical tunneling processes and defects that occur at the interfaces between different types of semiconductors and how these defects affect device characteristics.

In addition, SCAPS-1D is an inexpensive and fast alternative to performing the same type of experiments using laboratory techniques. Performing these types of experiments will take a significant amount of time and money, while using SCAPS-1D will allow the user to enter parameters digitally and automatically find the best possible answer. This provides an opportunity to rapidly design devices and to investigate the new materials. SCAPS-1D solves most of the main semiconductor equations that include electrons and holes, including the Poisson equation, continuity equations, and both current and voltage equations.

$$\frac{d^2\varphi(x)}{dx^2} = \frac{e}{\varepsilon_0 * \varepsilon_r}(p(x) - n(x) + N_D - N_A + \rho_P - \rho_n) \tag{1}$$

$$\frac{dJ_n}{dx} = G - R \tag{2}$$

$$\frac{dJ_p}{dx} = G - R \tag{3}$$

$$J_n = q\mu_n n\frac{d\varphi}{dx} + qD_n\frac{dn}{dx} \tag{4}$$

$$J_p = q\mu_p p\frac{d\varphi}{dx} - qD_p\frac{dp}{dx} \tag{5}$$

In this example, the dielectric constant of a vacuum, ε_0, a relative dielectric constant of ε_r; is the electron charge (e), n and p are electron and hole concentrations, such as N_D and N_A are densities of ionised donors (N_D) and acceptors (N_A) Electron and hole current densities (J_n and J_p) are described by recombination rates (R) and carrier generation rates (G), as well as their mobilities (μ_n and μ_p); along with their respective diffusion coefficients (D_n and D_p). The electric potential gradient can be established via Equation (1), which indicates the dependence of the electric potential gradient on the distribution of charge density with respect to electron and hole charges. Continuity equations are presented in Equations (2) and (3) and provide continuity for both electron (J_n) and hole (J_p) current densities, which are dependent upon their respective generation and recombination rates. Total current densities (with respect to both electrons and holes) are given by Equations (4) and (5) and consist of the total contribution of both drift and diffusion of the respective charge carriers. The direction that the carriers diffuse from regions of higher concentration to lower concentration is negative for holes, as they have negative charge; whereas electrons diffuse from regions of low concentration to more concentration.

3.3. Limitations of the SCAPS-1D Program

While SCAPS-1D is commonly used as a tool for modeling semiconductor components, it has a number of constraints that can affect how reliable results can be generated, and, in turn, can affect the usability of SCAPS-1D. To develop a model using SCAPS-1D, the user must make several assumptions regarding the idealized conditions under which the model is designed. For example, SCAPS-1D assumes that all layers of a semiconductor are “flat” and “uniform” in terms of their material properties (for example, composition, thickness, and crystal structure). In reality, there are many ways that a material's properties can vary within its layers (i.e., after undergoing defects due to manufacturing processes), and therefore these assumptions do not accurately reflect real-world systems. SCAPS-1D also assumes that all interfaces between layers are “perfectly flat”, but again this is not the case. Depending on the temperature, pressure and chemical environment in which a semiconductor is manufactured and processed, there may be defects and irregularities present at the interfaces between layers. These assumptions can result in discrepancies between computed and measured results when comparing complex or non-ideal systems. The user of SCAPS-1D must conduct proper experiments and use accurate and complete input parameters to obtain reliable results.

4. Modeling and Optimization of Sb_2Se_3 Solar Cells in SCAPS-1D

Modeling primarily aims to improve the PCE of the device. This is achieved by optimizing layer thicknesses, adjusting doping concentrations, reducing defect density, and optimizing series (R_s) and shunt (R_{sh}) resistances. Typically, two main architectures are used: superstrate and substrate. In the superstrate configuration, the layers are arranged sequentially on a transparent substrate (usually TCO on soda–lime glass): front contact, electron transport layer (ETL), absorber, hole transport layer (HTL), and back contact. In the substrate configuration, the order is reversed: glass, back contact, absorber, buffer (ETL), and transparent top layer. When these layers are stacked, band alignment occurs, which is explained by the Anderson model: if the electron affinity of the absorber χ_{abs} is greater than that of the buffer χ_{buf}, spike-like alignment is observed. If the spike is within the 0.3 eV range, electrons can easily transfer from the absorber to the buffer. When the value is higher, electron transport becomes inhibited, reducing the short-circuit current. If χ_{buf} is smaller than χ_{abs}, carrier recombination increases and the open-circuit voltage decreases. Therefore, selecting the optimal 0–0.3 eV spike-like alignment is essential. SCAPS mainly evaluates device performance based on band alignment. The most commonly used ETL material paired with Sb_2Se_3 is CdS. It is a natural starting candidate due to its useful properties: direct bandgap $E_g \approx 2.42$ eV, absorption coefficient 10^4 cm^{-1}, and charge-carrier mobility of 10^2 cm^2 $V^{-1}s^{-1}$ [7]. An important advantage of CdS is that it has already been successfully used as a buffer layer in CdTe and CIGS technologies [23]. Researchers have also proposed improved buffer layers. The following sections discuss various buffer layers, n^+ layers, additional p^+ layers on the absorber, combinations of n^+ and p^+ layers, and perovskite layers that significantly enhance the efficiency of the device.

4.1. Effect of a Single p–n Junction Structure in Sb_2Se_3 based Solar Cells

Working with SCAPS, Ling-Yan Lin and collaborators produced modeling work on Sb_2Se_3/CdS thin-film photovoltaic devices. The study revealed that optimal absorber and buffer layer thicknesses for such devices were found to be 600 nm and 60 nm, respectively. With a defect density of 10^{17} cm^{-3} and 10^8 cm^{-2} for the absorber and absorber-interface respectively, it was found that the devices could PCE as high as 16.5 % [11]. In the work performed by Mamta and colleagues, thin film CdS/Sb_2Se_3 solar cells were fabricated using a thermal evaporative deposition technique with absorber thicknesses of 372 nm and 640 nm. According to the results from SCAPS modeling, the devices exhibited efficiencies of 0.96% and 1.36% for these respective thicknesses and if the series and shunt resistances are properly adjusted and the absorber band gap is reduced from 1.47 eV to 1.2 eV, the maximum efficiency of the devices can reach up to approximately 11.27% [24]. Ahmed Shaker and co-workers ran SCAPS simulations on hybrid hetero-junction and homojunction solar cells based on Sb_2Se_3, and reported maximum PCE values of 7.75%, 10.08%, and 8.79% when the cells were based on CdS, ZnOS, and homojunctions respectively. They established the following optimized parameters in their models for CdS and ZnOS-based cells: n-region x_n = 75nm, $N_D = 1\times10^{17}$ cm^{-3}, p-region x_p = 350 nm, $N_A = 4\times10^{16}$ cm^{-3}. A typical homojunction Solar Cell has x_n = 40 nm, a doping of $N_D = 5\times10^{17}$ cm^{-3}, a p-region width x_p = 400 nm, and an N_A of 10^{16} cm^{-3}. Compared to Heterojunctions, Homojunctions have no interface between dissimilar layers, resulting in lower recombination and shorter transport layers that provide better reliability [25]. Raman Kumari

and colleagues used SCAPS-1D to model a Mo/Sb_2Se_3/ZnSe/Al device, with a buffer layer thickness of 100 nm and an absorption layer thickness of 1.5 µm. In this study, the maximum efficiency for a radiative recombination coefficient of 1×10^{-11} cm^3/s was accomplished using an absorber carrier concentration of 3.5×10^{17} cm^3 [26]. The use of the Cu Sandwich Method (Cu/Sb_2Se_3/Cu) to create Sb_2Se_3 by sequentially depositing Sb and Se followed by annealing at various temperatures has resulted in an X-ray Diffraction (XRD) and Field Emission Scanning Electron Microscopy (FE-SEM) analysis indicating a transition from the (hk0) plane to the (hk1) plane, with the nanotubes transforming to a polygonal form as the annealing temperature increases. The estimated bandgap for the copper sandwich Sb_2Se_3 sample, using annealing at 450ºC, was 1.04 eV, and the carrier concentration in the Sb_2Se_3 layer was 3.1×10^{15} cm^{-3}. A heterojunction solar cell was constructed with the 450°C annealed Sb_2Se_3 on top of a Glass/Ni/p-Sb_2Se_3/n-ZnSe/ITO/Al substrate and simulated using SCAPS-1D. This device produced an efficiency of 21.51%, an open-circuit voltage of 0.718 V, a current density of 43.33 mA cm^{-2}, and a Fill Factor of 69.14% [27]. The photovoltaic parameters of these single p-n junction Sb_2Se_3-based solar cells are summarized in Table 1.

Table 1. Photovoltaic parameters of single p-n junction **Sb_2Se_3**-based solar cells

no.	Sructure	χ (absorber/buffer)	E_g (absorber/buffer)	V_{oc} (V)	J_{sc} (mA/cm²)	FF (%)	PCE (%)	Reference
1	Au/Sb_2Se_3/CdS/FTO	3.9/4.2	1.06/2.4	0.40	41.86	74.08	16.5	[11]
2	Ag/Sb_2Se_3/CdS/ITO	4.04/4.2/4.5	1.47/2.4/3.7	0.74	18.07	83.62	11.27	[24]
3	Au/Sb_2Se_3/ZnOS/FTO	4.04/4.5	1.2/3.14	0.70	33.29	70.13	16.51	[25]
4	Mo/Sb_2Se_3/ZnSe/Al	4.04/4.09	1.2/2.7	0.85	34	83.61	24.01	[26]
5	Mo/Sb_2Se_3/ZnSe/ITO/Al	4.04/4.09/4.5	1.2/2.7	0.71	43.33	69.14	21.5	[27]

The UPS/HAXPES value obtained by Don et al. [28], was 5.13 eV for Sb_2Se_3 this would indicate a VBM of -5.13 eV in relation to a vacuum level. Our SCAPS simulations detected that the VBM of Sb_2Se_3 is –5.24 eV which falls within the conventional experimental uncertainty (±0.1 eV) and may be seen as an approximated adjustment of our model to compensate for the quality of films and surface termination, as well as the optimization of the band alignment of a particular device. Additionally, the SCAPS results produced by our model indicate that if the absorber thickness is held between 800 nm and 1.5 µm, with a defect density in the range of 10^{14} cm^{-3}, with carrier mobilities from 15-42 cm^2 $V^{-1}s^{-1}$, and the back-contact work function is about 4.8 eV with radiative recombination coefficients of 10^{-11} cm^3/s then the efficiency of the simulated device should be in the vicinity of 16.5-24%. The results of this research indicate that the primary method for increasing conversion efficiency will be to create differences between the conduction band and valence band. Additionally, SCAPS simulation studies performed for the integration of a ZnSe buffer layer into the overall growth scheme have shown that an enhancement of efficiency is also possible with the addition of a ZnSe buffer layer due in large measure to the superior lattice match (on the order of 2.52-3.94%) of the Sb_2Se_3 and ZnSe materials, along with the bandgap, (2.70 eV) and the electron affinity (~4.09 eV) of ZnSe, both of which combine to provide lower rates of interfacial recombination and higher rates of carrier extraction from the system. These are the reasons why ZnSe is a candidate for use as a buffer layer in next-generation Sb_2Se_3 photovoltaic cells built using a technology similar to that illustrated in Figure 3.

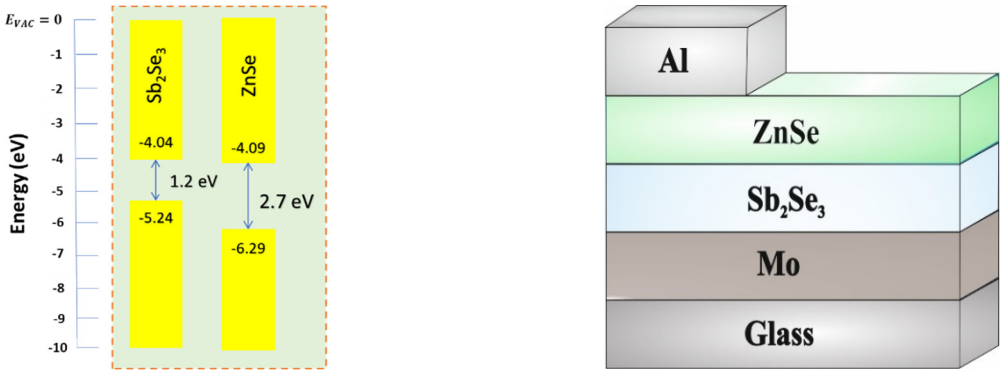

Figure 3. Energy band diagram of Sb_2Se_3 /ZnSe structure solar cell

4.2. Effect of a p^+ Layer in Sb_2Se_3 based Solar Cells

Basra Sultana et al. utilized SCAPS-1D simulations to optimize a Cu/FTO/CdS/SnSe/Sb_2Se_3/Au solar device (where SnSe serves as the primary absorber layer and Sb_2Se_3 serves as a secondary absorber). The efficiency of the device (Cu/FTO/CdS/SnSe/Au) prior to optimization was: PCE=26.15%, V_{oc}=0.79 V, J_{sc}=36.36 mA/cm^2, and FF=85.94%. The optimized device (Cu/FTO/CdS/SnSe/Sb_2Se_3/Au) had improved performance characteristics due to improved absorption capabilities and charge-carrier separation at the SnSe/Sb_2Se_3 interface [29]. Specifically, the optimized device demonstrated improvements to a PCE of 28.18%, V_{oc} of 0.84 V, J_{sc} of 38.42 mA/cm^2, and FF of 86.57% as compared to the non-optimized device. Aside from investigating the performance enhancement at the SnSe/Sb_2Se_3 interface, the investigation determined

that further performance enhancements could be achieved using TiO_2 buffer layers and Cu_2O BSF layers incorporated into the Sb_2Se_3 solar devices. In this study, the optimal thicknesses for the absorber and BSF layers were determined to be 500 nm and 20 nm, respectively; carrier concentrations were determined to be 1×10^{16} and 1×10^{18} cm^{-3} respectively, the defect density for both layers was 1×10^{14} cm^{-3}, and interface defect densities were determined to be 1×10^{13} cm^{-2} for the absorber and 1×10^{12} cm^{-2} for the BSF layers. The previous sections describe the parameters and calculations used to determine the output characteristics for this device. These parameters include operating temperature, electron affinity, E_g, surface recombination velocity, series resistance, and shunt resistance. Based on the optimized parameters of this Al/ITO/TiO_2/Sb_2Se_3/Cu_2O/Ni double-junction heterostructure, a PCE of 32.102% was achieved, with J_{sc} of 37.49 mA/cm^2, V_{oc} of 1.024 V, and FF of 83.59% [17]. S.H. Liu et al. proposed a solar cell with the following configuration: Al/FTO/CdS/Sb_2Se_3/Sb_2S_3/Mo. During the optimization process, the following parameters were varied: operating temperature, series resistance, shunt resistance, doping concentration, bulk defect density, the work function of the back-contact metal, and absorber layer thickness. The optimized combination of the Sb_2Se_3 absorber with the addition of an Sb_2S_3 layer resulted in a PCE of 28.91% with a 1 μm thick Sb_2Se_3 absorber layer; a 0.05 μm thick Sb_2S_3 BSF layer; and a carrier concentration of 1×10^{17} cm^{-3} in the Sb_2Se_3 [30]. Mutaz Salih Hasan Aljuboori and coworkers conducted a study of a solar cell with Glass/Mo/$CuSbS_3$/Sb_2S_3/CdS/i:ZnO/Al:ZnO which aimed to increase the maximum conversion efficiency of the cell by changing the thickness of the Sb_2S_3 layer from 1 to 3.5 μm. The maximum conversion efficiency was achieved with an absorber thickness of 3.5 μm resulting in a conversion efficiency of 23.14% and a fill factor of 87.52%. They also tested various materials to use as a secondary absorber layer lying between the primary absorber and the buffer layer including $MAPbI_3$, Sb_2Se_3, CZTS and CZTSe. They found that Sb_2Se_3 provided the highest conversion efficiency with a conversion efficiency of 27.01% and a fill factor of 85.12% after optimising the device [31]. Ferdous Rahman and coworkers also investigated the performance of Sb_2Se_3 solar cells when utilising a WS_2 buffer layer and a CZTSe BSF layer within a simulated structure (Al/FTO/WS_2/Sb_2Se_3/CZTSe/Pt) modelled using SCAPS-1D simulation software. For the purpose of maximizing the possible PCE, careful optimization of numerous parameters was performed, including the thickness of the absorber, buffer layer, donor and acceptor concentrations (N_D and N_A, respectively), the density of defects (N_t), and the series and shunt resistances (R_s and R_{sh} respectively). Without the addition of a p^+ layer in the proposed device described above, the measured data indicated a PCE of 28.20%, FF of 86.56%, V_{oc} of 0.85 V, and J_{sc} of 38.40 mA/cm^2. The PCE increased to 31.52%, J_{sc} to 38.49 mA/cm^2, V_{oc} to 0.94 V, and FF to 86.61% when a p^+ layer was added [32]. Studies have shown that by adding p+ dopants to Sb_2Se_3 based solar cells, PCE can be greatly improved. A high acceptor density located close to the back electrode of the solar cell eliminates or at least reduces any chance for hole recombination occurring at the back side of the spreader, thus leading to a higher Voc and improved PCE. Furthermore, when conduction and valence bands are aligned better, the diffusion length of charge carriers (holes and electrons) is increased, in turn leading to an increased J_{sc}. The maximum reported PCE obtained during this analysis was found to be 32.1%, with a vertical orientation of Cu_2O as the back surface field layer. The parameters for this process were optimised in this case by using the following: the thickness of both Sb_2Se_3 and Cu_2O layers were set at 500 nm and 20 nm, 1×10^{16} cm^{-3} and 1×10^{18} cm^{-3} were the carrier concentrations for the Sb_2Se_3 and Cu_2O respectively, a defect density of 1×10^{14} cm^{-3} and the interface defect densities for both materials were set at 1×10^{13} cm^{-2} for Sb_2Se_3 and 1×10^{12} cm^{-2} for Cu_2O. A representation of the energy band diagram for these structures can be found in Figure 4. Based on the results from 1D SCAPS studies on these systems, several ways to enhance photovoltaic performance include using BSF engineering by introducing an additional absorber for additional depth of light absorption, increasing the selectivity of the back contact, and optimising the geometry of the back-contact system to facilitate increased charge carrier transport. BSF materials are Cu_2O, Sb_2S_3, CZTSe, and alternative buffer materials such as ZnSe/ZnOS/TiO_2 for replacing CdS based buffers. The introduction of BSF materials greatly reduces the SRH recombination at the back surface. Additionally, optimising the conduction band offset (CBO) and valence band offset (VBO) in the energy band diagram improves selectivity of charge carriers and the second absorber offers a larger optical volume for light. These high PCE values are derived from 1D modelling under ideal circumstances; the actual lifetime of devices will be impacted by grain boundary transport and material anisotropy. The photovoltaic parameters of these p+-doped Sb_2Se_3-based solar cells are summarized in Table 2.

Table 2. Photovoltaic parameters of p^+-doped Sb_2Se_3-based solar cells.

no.	Sructure	χ (absorber/buffer)	E_g (absorber/buffer)	V_{oc} (V)	J_{sc} (mA/cm²)	FF (%)	PCE (%)	Reference
1	Au/Sb_2Se_3/SnSe/CdS/FTO /Cu	4.4/4.5/4.2	1.2/1.2/2.4	0.84	38.42	86.57	28.18	[29]
2	Ni/Cu_2O/Sb_2Se_3/TiO_2/ ITO/Al	3.2/4.16/4/4	2.2/1.2/3/3.2	1.02	37.49	83.59	32.10	[17]
3	Mo/Sb_2S_3/Sb_2Se_3/CdS/ FTO/Al	4.4/4.2	1.2/3.2	0.78	43.22	85.4	28.91	[30]
4	Mo/$CuSbS_3$/Sb_2Se_3/Sb_2S_3/ CdS/ZnO/ Al:ZnO	4.4/4.5	1.2/2.7	1.01	31.23	85.12	27.0	[31]
5	Pt/CZTSe/Sb_2Se_3/WS_2/ FTO/Al	4.1/4.16/3.95/4	1.4/1.2/2.2/3.6	0.94	38.49	86.61	31.5	[32]

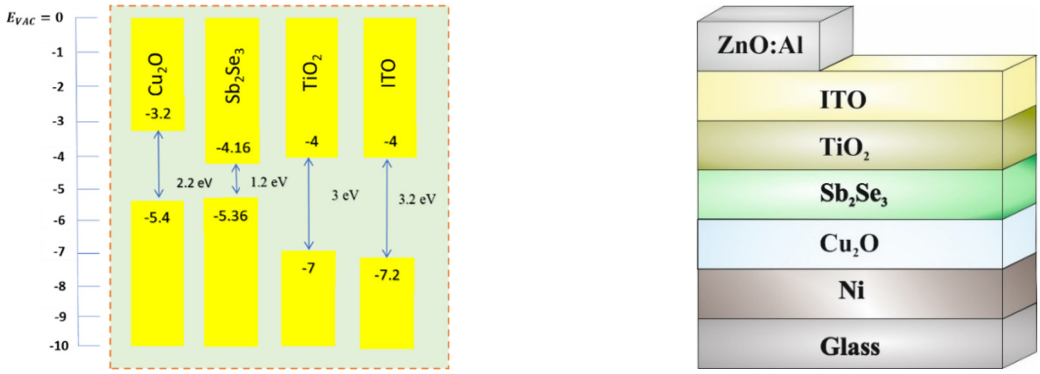

Figure 4. Structural and energy band diagram of p^+-Cu_2O/Sb_2Se_3 based solar cells

4.3. Effect of n^+ Doping in Sb_2Se_3 Based Solar Cells

The collaborative work of K.K Maurya and others provides important insight using SCAPS-1D simulations to demonstrate the key factors affecting the overall efficiency of Sb_2Se_3 based solar cells. The simulations identified three key factors related to the performance of the devices, which are use of dual buffer layers; the optimum conditions under which the devices operate; and lastly the selection of a back contact with a high work function. The authors first simulated an Sb_2Se_3/CdS/ZnO structure using CdS as the main buffer layer and ZnO as the second buffer layer. The effect of the CdS and ZnO on the photovoltaic performance Parameters (V_{oc}, J_{sc}, FF, and PCE) while the thickness of the absorber layer was 0.8µm and the temperature was set to 200K as it was noted increased temperatures lower the overall performance due to the negative impact of elevated temperatures on the mobilities of electrons and holes. When the radiative recombination coefficient is less than 10^{-8} cm^3/s and the back contact work function is at 5.1 eV, this structure provides an efficiency of 27.84% [33]. In their next paper, the authors show a greater efficiency of the Sb_2Se_3 devices can reach a higher efficiency by incorporating the dual buffer layers of CdS/ZnS. The maximum PCE obtained was 22.22% when the thicknesses of each buffer were set to 20 and 60 nm respectively. The authors have also shown that an optimum back-contact work function can be achieved if it exceeds 4.8 eV at the optimum temperature of 280K for Sb_2Se_3 to achieve 23.49% efficiency [34]. The results from this study demonstrate a theoretical limit to increasing the efficiency of Sb_2Se_3-based devices; the additions of both an additional buffer and n^+ layer provide a method of achieving this limit. The insertion of a n^+ layer will produce a corresponding improvement in the energy-band alignment due to the increase in concentration of electrons at the back contact which was shown in Figure 5. Enhanced electron concentration allows for enhanced accumulation and transportation of electrons toward the front contact and explains why solar cells that include an n^+ layer are capable of achieving much greater efficiency compared to devices based on a single p–n junction (as shown in Table 3).

Table 3. Photovoltaic parameters of n^+ doped Sb_2Se_3 based solar cells.

no.	Sructure	χ (absorber/buffer)	E_g (absorber/buffer)	V_{oc} (V)	J_{sc} (mA/cm²)	FF (%)	PCE(%)	Reference
1	Au/Sb_2Se_3/CdS/ZnO/ Al	4/4.2/4.4	1.2/2.4/3.3	0.98	42.4	66.81	27.8	[33]
2	Au/Sb_2Se_3/CdS/ZnS/Z nO/Al	4.04/4.2/4.5	1.2/2.4/3.5	0.77	35.5	85.32	23.49	[34]

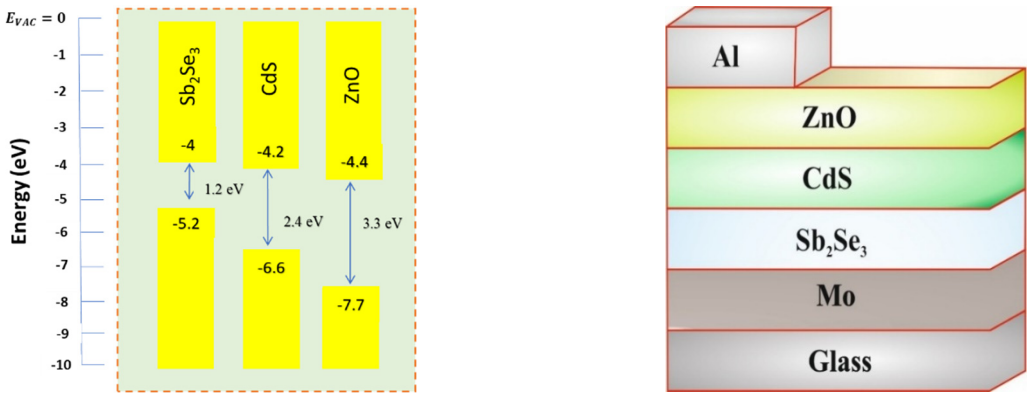

Figure 5. Energy band diagram of **Sb_2Se_3** /CdS/ n^+-ZnO structure solar cell

4.4. Effect of p^+/n^+ Doping in Sb_2Se_3 Based Solar Cells

In their laboratory experiments, Faisal Baig and his associates obtained an experimental efficiency of 6.39 for the structure Au/PbS/Sb_2Se_3/CdS/ITO; thereafter, SCAPS was simulated by substituting the PbS layer with Cu_2O (theoretical efficiency = 8.42%); SCAPS efficiency increased to 13.2% when replacing CdS with In_2S_3 (2.9 eV band gap and 3.85 eV electron affinity); based on these results, a new configuration for this solar cell was devised (CNT/Cu_2O/Sb_2Se_3/In_2S_3/ITO). The new structure, which has the configuration of Cu_2O as the HTL, In_2S_3 as the ETL, and CNTs as the back contact, was developed to further enhance the efficiency of this type of solar cell [12]. Abdelaziz Ait Abdelkadir and his co-researchers conducted a theoretical modeling study for the characterization of experimental Sb_2Se_3 solar cells. It was found that an efficiency of 16.62% was attained when the Sb_2Se_3 layer was 1.2 µm thick, carrier concentration was 10^{15} cm^{-3}, bulk defect density was 10^{13} cm^{-3}, and interface defect density was 10^{10} cm^{-2}. The device performance increased when an n-GaAs layer (100 nm thick) was added between the n-CdS and p-Sb_2Se_3, along with a p^+ Cu_2O HTL (100 nm thick) used as a BSF. This optimized arrangement produced more efficient electron transport and diffusion from the Sb_2Se_3 layer to the CdS layer, resulting in improved device performance. The addition of the p^+ Cu_2O HTL at the back contact also provided a greater potential barrier that limited recombination of the charge carriers at the back contact. The resulting device structure, ITO/CdS/GaAs/Sb_2Se_3/Cu_2O/Au, achieved an efficiency of 19.60%, with a J_{sc} of 36.38 mA/cm^2, a V_{oc} of 0.73 V, and a FF of 73.47% [35]. Z. Dahmardeh et al. simulated a Sb_2S_3/Sb_2Se_3 solar cell and reported PCE of 22.2% using absorber layer thicknesses of 420 nm and 1020 nm, respectively [36]. Shriya Sakul Bal et al. also studied a solar cell with a different structure (Mo/Sb_2Se_3/Sb_2S_3/CdS/ZnO/ZnO:Al), using 500 nm of Sb_2S_3 and 1000 nm of Sb_2Se_3 for the absorber layers. The thickness of the CdS/ZnO buffer was determined to be optimal at 80 nm for CdS and 50 nm for ZnO. After fully optimized, the maximum efficiency of 13.2% was achieved; with FF of 78.64%, J_{sc} of 29.33 mA/cm^2, and V_{oc} of 0.58 volts [37]. When combined p^+/n^+ doped Sb_2Se_3 photovoltaic cells are compared with single p-n junction a Sb_2Se_3 photovoltaic cell, the efficiencies were significantly lower. The decrease in efficiency is attributed to two main factors: (1) the additional layers create an increase in the number of recombination centres at the different interface, which reduces the V_{oc}, and (2) the increase in the total thickness of the device decreases the total light being absorbed and also the number of photons that can penetrate into the absorber layer and ultimately decrease the J_{sc} (see Table 4 and Figure 6).

Table 4. Photovoltaic parameters of p^+/n^+-layers added Sb_2Se_3-based solar cells

no.	Structure	χ (absorber/buffer)	E_g (absorber/buffer)	V_{oc} (V)	J_{sc} (mA/cm^2)	FF (%)	PCE (%)	Reference
1	CNT/Cu_2O/Sb_2Se_3 /InS_3/ITO	3.2/4.15/4.25/4.5	2.2/1.06/2.9/3.6	0.67	26.84	79.74	13.2	[12]
2	Au/Cu_2O/Sb_2Se_3/ GaAs/CdS/ITO	3.2/4.18/4.07/4.4/4.5	2.2/1.19/1.43/2.42/3.6	0.73	36.38	73.47	19.6	[35]
3	Mo/Sb_2Se_3/Sb_2S_3/ CdS/ZnO/ZnO:Al	4.04/4/4.2/4.5	1.2/1.67/2.4/3.3	1.02	20.15	59.58	22.2	[36]
4	Mo/Sb_2Se_3/Sb_2S_3/ CdS/ZnO/ZnO:Al	3.7/3.7/4.2/4.5	1.08/1.62/2.4/3.3	0.58	29.33	78.64	13.2	[37]

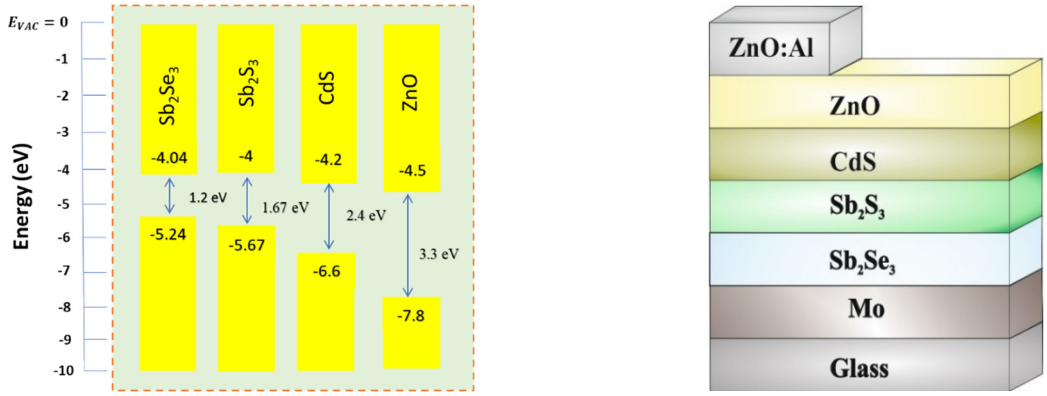

Figure 6. Energy band diagram of p^+/n^+-layers added Sb_2Se_3 based solar cells

4.5. Effect of Perovskite Incorporation in Sb_2Se_3 Based Solar Cells

Masood Mehrabian and co-workers simulated a multi-layer dual-absorber solar cell with the structure FTO/CdS/Sb_2Se_3/$CuInSe_2$/Au, achieving PCE = 5.55%, FF = 54.68%, J_{sc} = 27.54 mA/cm², and V_{oc} = 0.36 V. By replacing the CdS ETL with a C_{60} layer, the photovoltaic performance improved to PCE = 9.20%, FF = 67.78%, J_{sc} = 27.38 mA/cm^2, and V_{oc} = 0.49 V (Table 5). Furthermore, by incorporating a $CsSn_{0.5}Ge_{0.5}I_3$ perovskite absorber layer, the efficiency increased to 11.42%. Although the maximum recombination rate in the CdS layer was about one order lower than in the C_{60} layer, the smaller bandgap (E_g) of C_{60} compensated for its higher recombination rate, contributing to improved PCE

[38]. In another study, Mousaab Belarbi used $KSnI_3$ perovskite layer in FTO/SnS_2/$KSnI_3$/Sb_2Se_3/Pt device and replaced the Pt back contact with tungsten (W). When the absorber thickness was 0.9 µm, donor and acceptor concentrations were 10^{17} cm^{-3} and 10^{20} cm^{-3}, the operating temperature was 280 K, and the $KSnI_3$ bandgap was 1.74 eV, the device performance improved significantly. Jsc increased from 13.79 to 26.08 mA/cm^2, FF from 69.07% to 76.25%, and PCE from 12.72% to 23.85% [39]. Arslan Ashfaq and co-workers performed numerical simulations of p-Sb_2Se_3/n-$BaZrS_3$ heterojunction solar cells. Compared to lead-based chalcogenide perovskites, n-$BaZrS_3$ is more stable, non-toxic, and suitable for thin-film solar cell applications as a sulfur-based chalcogenide material. In their study, the photovoltaic parameters achieved were PCE = 32.87%, FF = 88.22%, J_{sc} = 36.88 mA/cm^2, and V_{oc} = 1.01 V. The best performance was obtained when the p-Sb_2Se_3 absorber layer thickness was 7000 nm, the bandgap 1.15 eV, and carrier concentration 10^{20} cm^{-3}. For $BaZrS_3$, the optimal parameters were thickness of 100 nm, carrier concentration of 10^{17} cm^{-3}, and a bandgap of 1.76 eV. One advantage of these perovskites is their strong ionic coordination, which enhances the Coulomb attraction between positive and negative ions [40]. Jing Wu and co-workers simulated Sb_2Se_3/$MAPbI_3$ solar cell using SCAPS-1D, analyzing absorber layer thicknesses of Sb_2Se_3 and methylammonium lead iodide ($MAPbI_3$), the thickness and doping concentration of the n-type buffer layer, as well as the bulk defect densities of Sb_2Se_3 and $MAPbI_3$. In addition, the effects of defect density at the Sb_2Se_3/$MAPbI_3$ and $MAPbI_3$/TiO_2 interfaces on device efficiency were investigated. The optimal absorber thicknesses were found to be 0.6 µm for Sb_2Se_3 and 0.7 µm for $MAPbI_3$. Further analysis revealed that within optimized parameters, the donor concentration (N_D) of the TiO_2 buffer layer reached 10^{18} cm^{-3}, while its optimal thickness was 0.05 nm. Moreover, the bulk defect densities of Sb_2Se_3 and $MAPbI_3$ should be 10^{13} cm^{-3} or lower, and the interface defect densities should be 10^{11} cm^{-2} or lower to achieve an efficiency of 21.90% [41]. The significant enhancement of photovoltaic performance through perovskite incorporation in Sb_2Se_3 based solar cells can be seen in Table 5 and Figure 7. Notably, the inclusion of $BaZrS_3$ layer demonstrated efficiency values approaching the Shockley-Queisser limit, with well-aligned energy band matching.

Table 5. Photovoltaic parameters of perovskite integrated **Sb_2Se_3** based solar cells

no.	Sructure	χ (absorber/buffer)	E_g (absorber/buffer)	V_{oc} (V)	J_{sc} (mA/cm^2)	FF (%)	PCE (%)	Reference
1	FTO/C_{60}/$CsSn_{0.5}Ge_{0.5}I_3$/Sb_2Se_3/$CuInSe_2$/Au	3.9/3.9/3.9/4.3	1.7/1.5/1.06/1.04	0.49	27.38	67.78	11.4	[38]
2	FTO/SnS_2/$KsnI_3$/Sb_2Se_3/W	4/4.16/3.44/4.04	3.5/2.3/1.84/1.2	1.19	26.08	76.25	23.85	[39]
3	Mo/Sb_2Se_3/$BaZrS_3$/FTO	4.05/4.1/4.4	1.2/1.76/3.2	1.01	36.88	88.22	32.8	[40]
4	Sb_2Se_3/$MAPbI_3$/TiO_2	3.9/3.9/3.9	1.06/1.5/3.1	0.69	43	78.5	21.9	[41]

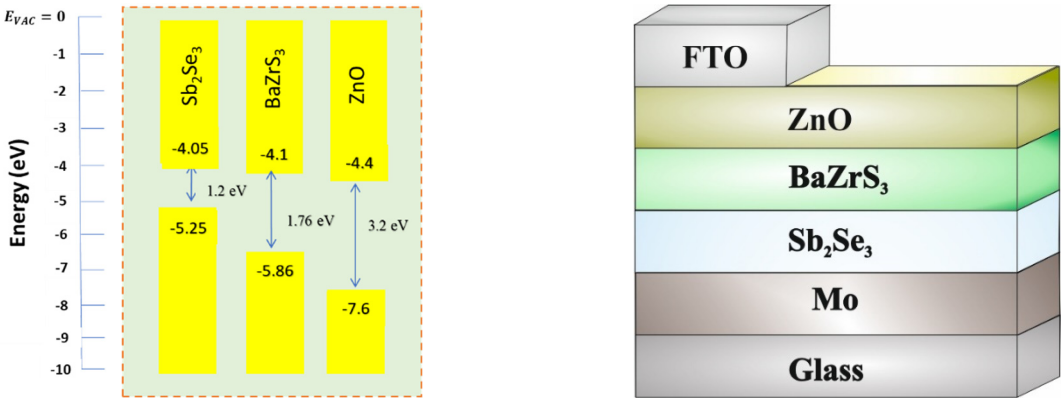

Figure 7. Energy band diagram of Perovskite thin layer added Sb_2Se_3 based solar cells

5. CONCLUSIONS

By combining SCAPS-1D simulations with experimental analyses, significant progress has been achieved toward optimizing Sb_2Se_3 based thin-film solar cells. In this study, the optical, structural, and electronic properties of Sb_2Se_3 were comprehensively investigated, and several advanced device configurations including single p-n junctions, p^+-doped, n^+-enhanced architectures, p^+/n^+ co-doped structures, and perovskite-integrated heterojunctions were analyzed. The modeling results demonstrated that high efficiencies can be achieved with absorber layer thicknesses ranging from 800 nm to 1.5 µm, low bulk defect densities on the order of 10^{14} cm^{-3}, interface defect densities of 10^{11} cm^{-2}, appropriate carrier mobilities, and favorable energy band alignment. One important finding was the substantial benefit of incorporating a ZnSe layer as the buffer material. This improvement results from its favorable band alignment, electron affinity, and excellent lattice compatibility with Sb_2Se_3. Furthermore, the introduction of a p^+ layer was shown to enhance device efficiency. With a high acceptor concentration (10^{18} cm^{-3}) in the p^+ region and a very thin (20 nm) layer, hole recombination near the back electrode was significantly suppressed, leading to higher open-circuit voltage. Improved conduction and valence band alignment also increased the diffusion lengths of electrons and holes, thereby enhancing the short-circuit current. Among all investigated

configurations, the Cu_2O BSF (back-surface field) layer achieved the highest efficiency of 32.1%. Cu_2O, Sb_2Se_3, and CZTSe were identified as promising alternative BSF materials, all effectively reducing SRH recombination at the rear interface. It should be noted that the reported efficiency values are based on 1-D simulation assumptions involving ideal interfaces and simplified defect densities; therefore, real devices must account for grain-boundary transport and anisotropy effects. The study further showed that incorporating an additional n^+ layer not just a single buffer can theoretically improve device performance, as confirmed both by improved band alignment and experimental observations demonstrating enhanced electron collection at the front contact. In contrast, the use of combined p^+/ n^+ doping led to reduced efficiencies. This reduction is attributed to an increased number of interfaces, which introduce additional recombination centers and thereby lower the open-circuit voltage. Moreover, excessive total thickness decreases light absorption, reducing photon penetration into the absorber and subsequently lowering the short-circuit current. Perovskite incorporation, particularly the inclusion of $BaZrSe_3$ layer, significantly improved device performance. Structures employing this material demonstrated efficiencies close to the Shockley-Queisser theoretical limit. These results were enabled by nearly ideal band alignment and exceptional lattice matching between $BaZrSe_3$ and Sb_2Se_3 (with only ~0.2% mismatch). In summary, Sb_2Se_3 based solar cells when designed with careful consideration of defect passivation, interface engineering, and advanced heterostructure configurations hold strong promise as next-generation high-efficiency photovoltaic technologies.

Funding

This work was supported by the Basic Research Program of the Academy of Sciences of the Republic of Uzbekistan

Declaration of competing interest

The authors declare that they have no known competing financial interests or personal relationships that could have appeared to influence the work reported in this paper.

Data availability

Data will be made available on request.

Acknowledgements

The authors gratefully acknowledge Prof. M. Burgelman and the Department of Electronics and Information Systems, Ghent University, Belgium, for providing the SCAPS-1D software free of charge.

ORCID

K.M. Kuchkarov, https://orcid.org/0000-0002-2238-7205; **B.A. Ergashev,** https://orcid.org/0000-0001-9456-7961;
R.T. Yuldoshov, https://orcid.org/0000-0002-7886-1607; **M.P. Pirimmatov,** https://orcid.org/0009-0000-4829-7817;
R.R. Khurramov, https://orcid.org/0009-0008-1038-0138; **D.Z. Isakov,** https://orcid.org/0000-0003-4314-5683;
M.A. Makhmudov https://orcid.org/0009-0008-8836-0559; **Sh.M. Bobomuradov,** https://orcid.org/0009-0001-1338-3202;
A.S. Matmuradov, https://orcid.org/0009-0005-6121-6424; **A. Eshqorayev,** https://orcid.org/0009-0008-9022-5700

REFERENCES

[1] A.A.F. Husain, W.Z.W. Hasan, S. Shafie, M.N. Hamidon, and S.S. Pandey, "A review of transparent solar photovoltaic technologies," (2018). https://doi.org/10.1016/j.rser.2018.06.031

[2] Sadanand, P. K. Singh, S. Rai, P. Lohia, and D. K. Dwivedi, "Comparative study of the CZTS, CuSbS2 and $CuSbSe_2$ solar photovoltaic cell with an earth-abundant non-toxic buffer layer," Solar Energy, **222**, 2021, https://doi.org/10.1016/j.solener.2021.05.013

[3] S. Rühle, "Tabulated values of the Shockley-Queisser limit for single junction solar cells," Solar Energy, **130**, 2016, https://doi.org/10.1016/j.solener.2016.02.015

[4] A. Mavlonov, et al., "A review of Sb_2Se_3 photovoltaic absorber materials and thin-film solar cells," (2020). https://doi.org/10.1016/j.solener.2020.03.009

[5] C. Chen, et al., "Characterization of basic physical properties of Sb_2Se_3 and its relevance for photovoltaics," Frontiers of Optoelectronics, **10**(1), (2017). https://doi.org/10.1007/s12200-017-0702-z

[6] X. Wen et al., "Vapor transport deposition of antimony selenide thin film solar cells with 7.6% efficiency," Nat. Commun., **9**(1), (2018). https://doi.org/10.1038/s41467-018-04634-6

[7] Zhiqiang Li, "9.2%-efficient core-shell structured anti mony selenide nanorod array solar cells," Nat. Commun., **10**(1), (2019). https://doi.org/10.1038/s41467-018-07903-6

[8] H. Ning, et al., "Enhancing the efficiency of Sb_2Se_3 solar cells using dual-functional potassium doping," Solar Energy Materials and Solar Cells, **221**, (2021). https://doi.org/10.1016/j.solmat.2020.110816

[9] J. Lin, et al., "Crystallographic orientation control and defect passivation for high-efficient antimony selenide thin-film solar cells," Materials Today Physics, **27**, (2022). https://doi.org/10.1016/j.mtphys.2022.100772

[10] Rong Tang, "Heterojunction annealing enabling record open-circuit voltage in antimony triselenide solar cells," Advanced Materials, **34**(14), (2022). https://doi.org/10.1002/adma.202109078

[11] L. yan Lin, L. qin Jiang, Y. Qiu, and B. dian Fan, "Analysis of Sb_2Se_3/CdS based photovoltaic cell: A numerical simulation approach," Journal of Physics and Chemistry of Solids, **122**, (2018). https://doi.org/10.1016/j.jpcs.2018.05.045

[12] F. Baig, Y. H. Khattak, S. Beg, and B. M. Soucase, "Numerical analysis of a novel CNT/Cu_2O/Sb_2Se_3/In_2S_3/ITO antimony selenide solar cell," Optik (Stuttg.), **197**, (2019). https://doi.org/10.1016/j.ijleo.2019.163107

[13] Y. Chen, et al., "Importance of interfacial passivation in the high efficiency of Sb_2Se_3 thin-film solar cells: Numerical evidence," ACS Appl. Energy Mater. **3**(11), (2020). https://doi.org/10.1021/acsaem.0c01203

[14] S. R. Al Ahmed, A. Sunny, and S. Rahman, "Performance enhancement of Sb_2Se_3 solar cell using a back surface field layer: A numerical simulation approach," Solar Energy Materials and Solar Cells, **221**, (2021). https://doi.org/10.1016/j.solmat.2020.110919
[15] S. Abbas, et al., "Numerical Simulation of the Performance of Sb_2Se_3 Solar Cell via Optimizing the Optoelectronic Properties Based SCAPS-1D," Materials, **15**(18), (2022). https://doi.org/10.3390/ma15186272
[16] A. El Khalfi, L. Et-Taya, Y. Achenani, M. Sahal, L. Elmaimouni, and A. Benami, "Performance Evaluation of Sb_2Se_3-based Solar Photovoltaic Cells with Various ETL and Cu_2O as HTL by SCAPS-1D," Karbala International Journal of Modern Science, **9**(3), (2023). https://doi.org/10.33640/2405-609X.3303
[17] B. Sultana, A. T. M. S. Islam, M. D. Haque, and A. Kuddus, "Cu_2O-Enhanced Back Surface Field Empowers Selenium-Based TiO_2/ Sb_2Se_3 Thin Film Solar Cells to Achieve Efficiency over 32%," Applied Solar Energy (English translation of Geliotekhnika), **59**(6), (2023). https://doi.org/10.3103/S0003701X23601515
[18] N. W. Tideswell, F. H. Kruse, and J. D. McCullough, "The crystal structure of antimony selenide, Sb_2Se_3," Acta Crystallogr. **10**(2), (1957). https://doi.org/10.1107/s0365110x57000298
[19] K. Li et al., "One-Dimensional Sb2Se3 Enabling Ultra-Flexible Solar Cells and Mini-Modules for IoT Applications," Nano Energy, **86**, 106101 (2021). https://doi.org/10.1016/j.nanoen.2021.106101
[20] K. Momma, and F. Izumi, "VESTA 3 for three-dimensional visualization of crystal, volumetric and morphology data," J. Appl. Crystallogr. **44**(6), (2011). https://doi.org/10.1107/S0021889811038970
[21] Y. Yan, et al., "Physics of grain boundaries in polycrystalline photovoltaic semiconductors," Journal of Applied Physics, **117**, 112807 (2015). https://doi.org/10.1063/1.4913833
[22] B. Zhang, and X. Qian, "Competing Superior Electronic Structure and Complex Defect Chemistry in Quasi-One-Dimensional Antimony Chalcogenide Photovoltaic Absorbers," ACS Appl. Energy Mater. 5(1), 1 (2022). https://doi.org/10.1021/acsaem.1c03023
[23] J. Ramanujam, and U.P. Singh, "Copper indium gallium selenide based solar cells - A review," **10**(6), 1306–1319 (2017). https://doi.org/10.1039/c7ee00826k
[24] Mamta, R. Kumari, C. Yadav, R. Kumar, K. K. Maurya, and V. N. Singh, "Thermally Deposited Sb_2Se_3/CdS-Based Solar Cell: Experimental and Theoretical Analysis," Nanomaterials, **13**(6), (2023). https://doi.org/10.3390/nano13061135
[25] A. Shaker, M. S. Salem, and K. Deepthi Jayan, "Analysis and design of p-n homojunction Sb_2Se_3 solar cells by numerical simulation," Solar Energy, (242), (2022). https://doi.org/10.1016/j.solener.2022.07.035
[26] R. Kumari, M. Mamta, R. Kumar, Y. Singh, and V. N. Singh, "24% Efficient, Simple ZnSe/ Sb_2Se_3 Heterojunction Solar Cell: An Analysis of PV Characteristics and Defects," ACS Omega, **8**(1), (2023). https://doi.org/10.1021/acsomega.2c07211
[27] B. Srinivas, S. Babujani, G. H. Chandra, Y. P. V. Subbaiah, and M. Gupta, "Synthesis and characterization of Cu-sandwiched Sb_2Se_3 thin films and numerical simulation of p- Sb_2Se_3/n-ZnSe heterojunction solar cell," Opt. Mater. (Amst). **135**, (2023). https://doi.org/10.1016/j.optmat.2022.113289
[28] C. H. Don, *et al*., "Sb 5s2lone pairs and band alignment of Sb_2Se_3: a photoemission and density functional theory study," J. Mater. Chem. C Mater. **8**(36), (2020). https://doi.org/10.1039/d0tc03470c
[29] F. B. Sultana, "A new design and optimization of SnSe-based dual absorber solar cell with efficiency above 28%," Journal of Nanoparticle Research, **26**(8), (2024). https://doi.org/10.1007/s11051-024-06085-1
[30] S. H. Liu, J. R. Yuan, Y. Wu, X. H. Deng, and Q. M. Yu, "Numerical simulation of Sb_2Se_3-based solar cells," Chalcogenide Letters, **21**(3), (2024). https://doi.org/10.15251/CL.2024.213.229
[31] M. S. Aljuboori, "Enhancing Photoconversion Efficiency by Optimization of Electron/Hole Transport Interlayers in Antimony Sulfide Solar Cell using SCAPS-1D Simulation," Solar Energy and Sustainable Development, **13**(1), 97–113 (2024). https://doi.org/10.51646/jsesd.v13i1.175
[32] M. F. Rahman, A. Lubaba, L. Ben Farhat, S. Ezzine, M. H. Rahman, and M. Harun-Or-Rashid, "Efficiency enhancement above 31 % of Sb_2Se_3 solar cells with optimizing various BSF layer," Materials Science and Engineering: B, **307**, (2024). https://doi.org/10.1016/j.mseb.2024.117527
[33] Mamta, K. K. Maurya, and V. N. Singh, "Efficient Sb_2Se_3 solar cell with a higher fill factor: A theoretical approach based on thickness and temperature," Solar Energy, **230**, (2021). https://doi.org/10.1016/j.solener.2021.11.002
[34] Mamta, K. K. Maurya, and V. N. Singh, "Enhancing the performance of a Sb_2Se_3-based solar cell by dual buffer layer," Sustainability (Switzerland), **13**(21), (2021). https://doi.org/10.3390/su132112320
[35] A. Ait Abdelkadir, M. Sahal, E. Oublal, N. Kumar, and A. Benami, "New Sb_2Se_3-based solar cell for achieving high efficiency theoretical modeling," Opt. Quantum Electron. **55**(6), (2023). https://doi.org/10.1007/s11082-023-04797-7
[36] Z. Dahmardeh, and M. Saadat, "Exploring the potential of standalone and tandem solar cells with Sb_2S_3 and Sb_2Se_3 absorbers: a simulation study," Sci. Rep. **13**(1), (2023). https://doi.org/10.1038/s41598-023-49269-w
[37] S. S. Bal, A. Basak, and U. P. Singh, "Numerical modeling and performance analysis of Sb-based tandem solar cell structure using SCAPS – 1D," Opt. Mater. (Amst). **127**, (2022). https://doi.org/10.1016/j.optmat.2022.112282
[38] M. Mehrabian, "Numerical optimization of cesium tin-germanium triiodide/antimony selenide perovskite solar cell with fullerene nanolayer," Journal of Physics and Chemistry of Solids, **196**, (2025). https://doi.org/10.1016/j.jpcs.2024.112370
[39] M. Belarbi, "Numerical analysis of performance enhancement in $KSnI_3$-based perovskite solar cells with Sb_2Se_3 as a hole transport layer," Materials Science and Engineering: B, **313**, (2025). https://doi.org/10.1016/j.mseb.2024.117874
[40] A. f Ashfaq, "High-efficiency selenium and sulfurbased p- Sb_2Se_3/n-$BaZrS_3$ heterostructure solar cells: A SCAPS-1D simulation study," Journal of Physics and Chemistry of Solids, **199**, (2025). https://doi.org/10.1016/j.jpcs.2024.112490
[41] J. Wu, Z. Zhao, Z. Zhao, M. Zhang, Y. Bi, X. Li, and L. Zhang, "Simulation Analysis of Sb_2Se_3 Narrow Bandgap Hole Transport Layer in $MAPbI_3$ Perovskite Solar Cells," Metals & Materials Society, Mar. **54**, 3910–3923 (2025). https://doi.org/10.1007/s11664-025-11886-8

МОДЕЛЮВАННЯ ТА ОПТИМІЗАЦІЙНА ВАЛІДАЦІЯ ТОНКОПЛІВКОВИХ СОНЯЧНИХ ЕЛЕМЕНТІВ Sb_2Se_3 У ПРОГРАМНОМУ ЗАБЕЗПЕЧЕННІ SCAPS-1D

К.М. Кучкаров, Б.А. Ергашев, Р.Т. Юлдошов, М.П. Пірімматов, Р.Р. Хуррамов, Д.З. Ісаков, М.А. Махмудов, Ш.М. Бобомурадов, А.С. Матмуратов, А.І. Ешкораєв

Фізико-технічний інститут імені А.С. Азімова, вулиця Чингіза Айтматова, 2Б, Ташкент 100084, Узбекистан

У цьому аналітичному есе розглядається селенід сурми (Sb_2Se_3) як потенційний матеріал-кандидат для використання в якості тонкоплівкового фотоелектричного поглинача. Sb_2Se_3 забезпечив значні екологічні/економічні переваги, включаючи велике оптичне поглинання, регульовану ширину забороненої зони близько 1,13 еВ та відсутність токсичних елементів. У цьому дослідженні було проведено параметричне дослідження на основі платформи SCAPS-1D з метою визначення ідеальних конструкцій шарів, інтерфейсів, динаміки носіїв заряду та вирівнювання зон. Цей аналіз зосереджений на механізмах втрат, які обмежують фотоелектричну продуктивність, з метою ізоляції та розробки стратегій для пригнічення рекомбінації Шоклі-Ріда-Холла, поверхневої рекомбінації, різниці в зміщенні зон та ефектів внутрішньої дифузії. Результати надають практичні пропозиції щодо мінімізації втрат напруги, такі як мінімізація товщини поглинача/буфера, мінімізація густини акцептора, оптимізація зміщення зони провідності якомога ближче до нуля та мінімізація поверхневої рекомбінації та густини дефектів.

Ключові слова: *Sb_2Se_3; тонкоплівковий сонячний елемент; SCAPS-1D; теоретична модель; оптимізація параметрів; фотоелектрична ефективність*